Measurements of the Absolute Branching Fractions of $B^{\pm} \to K^{\pm} X_{c\bar{c}}$

J. P. Lees,[1] V. Poireau,[1] V. Tisserand,[1] E. Grauges,[2] A. Palano,[3] G. Eigen,[4] D. N. Brown,[5] Yu. G. Kolomensky,[5] M. Fritsch,[6] H. Koch,[6] T. Schroeder,[6] R. Cheaib,[7b] C. Hearty,[7a,7b] T. S. Mattison,[7b] J. A. McKenna,[7b] R. Y. So,[7b] V. E. Blinov,[8a,8b,8c] A. R. Buzykaev,[8a] V. P. Druzhinin,[8a,8b] V. B. Golubev,[8a,8b] E. A. Kozyrev,[8a,8b] E. A. Kravchenko,[8a,8b] A. P. Onuchin,[8a,8b,8c] S. I. Serednyakov,[8a,8b] Yu. I. Skovpen,[8a,8b] E. P. Solodov,[8a,8b] K. Yu. Todyshev,[8a,8b] A. J. Lankford,[9] B. Dey,[10] J. W. Gary,[10] O. Long,[10] A. M. Eisner,[11] W. S. Lockman,[11] W. Panduro Vazquez,[11] D. S. Chao,[12] C. H. Cheng,[12] B. Echenard,[12] K. T. Flood,[12] D. G. Hitlin,[12] J. Kim,[12] Y. Li,[12] T. S. Miyashita,[12] P. Ongmongkolkul,[12] F. C. Porter,[12] M. Röhrken,[12] Z. Huard,[13] B. T. Meadows,[13] B. G. Pushpawela,[13] M. D. Sokoloff,[13] L. Sun,[13,†] J. G. Smith,[14] S. R. Wagner,[14] D. Bernard,[15] M. Verderi,[15] D. Bettoni,[16a] C. Bozzi,[16a] R. Calabrese,[16a,16b] G. Cibinetto,[16a,16b] E. Fioravanti,[16a,16b] I. Garzia,[16a,16b] E. Luppi,[16a,16b] V. Santoro,[16a] A. Calcaterra,[17] R. de Sangro,[17] G. Finocchiaro,[17] S. Martellotti,[17] P. Patteri,[17] I. M. Peruzzi,[17] M. Piccolo,[17] M. Rotondo,[17] A. Zallo,[17] S. Passaggio,[18] C. Patrignani,[18,‡] B. J. Shuve,[19] H. M. Lacker,[20] B. Bhuyan,[21] U. Mallik,[22] C. Chen,[23] J. Cochran,[23] S. Prell,[23] A. V. Gritsan,[24] N. Arnaud,[25] M. Davier,[25] F. Le Diberder,[25] A. M. Lutz,[25] G. Wormser,[25] D. J. Lange,[26] D. M. Wright,[26] J. P. Coleman,[27] E. Gabathuler,[27,*] D. E. Hutchcroft,[27] D. J. Payne,[27] C. Touramanis,[27] A. J. Bevan,[28] F. Di Lodovico,[28] R. Sacco,[28] G. Cowan,[29] Sw. Banerjee,[30] D. N. Brown,[30] C. L. Davis,[30] A. G. Denig,[31] W. Gradl,[31] K. Griessinger,[31] A. Hafner,[31] K. R. Schubert,[31] R. J. Barlow,[32,§] G. D. Lafferty,[32] R. Cenci,[33] A. Jawahery,[33] D. A. Roberts,[33] R. Cowan,[34] S. H. Robertson,[35a,35b] R. M. Seddon,[35b] N. Neri,[36a] F. Palombo,[36a,36b] L. Cremaldi,[37] R. Godang,[37,∥] D. J. Summers,[37] P. Taras,[38] G. De Nardo,[39] C. Sciacca,[39] G. Raven,[40] C. P. Jessop,[41] J. M. LoSecco,[41] K. Honscheid,[42] R. Kass,[42] A. Gaz,[43a] M. Margoni,[43a,43b] M. Posocco,[43a] G. Simi,[43a,43b] F. Simonetto,[43a,43b] R. Stroili,[43a,43b] S. Akar,[44] E. Ben-Haim,[44] M. Bomben,[44] G. R. Bonneaud,[44] G. Calderini,[44] J. Chauveau,[44] G. Marchiori,[44] J. Ocariz,[44] M. Biasini,[45a,45b] E. Manoni,[45a] A. Rossi,[45a] G. Batignani,[46a,46b] S. Bettarini,[46a,46b] M. Carpinelli,[46a,46b,¶] G. Casarosa,[46a,46b] M. Chrzaszcz,[46a] F. Forti,[46a,46b] M. A. Giorgi,[46a,46b] A. Lusiani,[46a,46c] B. Oberhof,[46a,46b] E. Paoloni,[46a,46b] M. Rama,[46a] G. Rizzo,[46a,46b] J. J. Walsh,[46a] L. Zani,[46a,46b] A. J. S. Smith,[47] F. Anulli,[48a] R. Faccini,[48a,48b] F. Ferrarotto,[48a] F. Ferroni,[48a,**] A. Pilloni,[48a,48b] G. Piredda,[48a,*] C. Bünger,[49] S. Dittrich,[49] O. Grünberg,[49] M. Heß,[49] T. Leddig,[49] C. Voß,[49] R. Waldi,[49] T. Adye,[50] F. F. Wilson,[50] S. Emery,[51] G. Vasseur,[51] D. Aston,[52] C. Cartaro,[52] M. R. Convery,[52] J. Dorfan,[52] W. Dunwoodie,[52] M. Ebert,[52] R. C. Field,[52] B. G. Fulsom,[52] M. T. Graham,[52] C. Hast,[52] W. R. Innes,[52,*] P. Kim,[52] D. W. G. S. Leith,[52,*] S. Luitz,[52] D. B. MacFarlane,[52] D. R. Muller,[52] H. Neal,[52] B. N. Ratcliff,[52] A. Roodman,[52] M. K. Sullivan,[52] J. Va'vra,[52] W. J. Wisniewski,[52] M. V. Purohit,[53] J. R. Wilson,[53] A. Randle-Conde,[54] S. J. Sekula,[54] H. Ahmed,[55] M. Bellis,[56] P. R. Burchat,[56] E. M. T. Puccio,[56] M. S. Alam,[57] J. A. Ernst,[57] R. Gorodeisky,[58] N. Guttman,[58] D. R. Peimer,[58] A. Soffer,[58] S. M. Spanier,[59] J. L. Ritchie,[60] R. F. Schwitters,[60] J. M. Izen,[61] X. C. Lou,[61] F. Bianchi,[62a,62b] F. De Mori,[62a,62b] A. Filippi,[62a] D. Gamba,[62a,62b] L. Lanceri,[63] L. Vitale,[63] F. Martinez-Vidal,[64] A. Oyanguren,[64] J. Albert,[65b] A. Beaulieu,[65b] F. U. Bernlochner,[65b] G. J. King,[65b] R. Kowalewski,[65b] T. Lueck,[65b] I. M. Nugent,[65b] J. M. Roney,[65b] R. J. Sobie,[65a,65b] N. Tasneem,[65b] T. J. Gershon,[66] P. F. Harrison,[66] T. E. Latham,[66] R. Prepost,[67] and S. L. Wu[67]

(*BaBar* Collaboration)

[1] *Laboratoire d'Annecy-le-Vieux de Physique des Particules (LAPP), Université de Savoie, CNRS/IN2P3, F-74941 Annecy-Le-Vieux, France*
[2] *Universitat de Barcelona, Facultat de Fisica, Departament ECM, E-08028 Barcelona, Spain*
[3] *INFN Sezione di Bari and Dipartimento di Fisica, Università di Bari, I-70126 Bari, Italy*
[4] *University of Bergen, Institute of Physics, N-5007 Bergen, Norway*
[5] *Lawrence Berkeley National Laboratory and University of California, Berkeley, California 94720, USA*
[6] *Ruhr Universität Bochum, Institut für Experimentalphysik 1, D-44780 Bochum, Germany*
[7a] *Institute of Particle Physics, Vancouver, British Columbia V6T 1Z1, Canada*
[7b] *University of British Columbia, Vancouver, British Columbia V6T 1Z1, Canada*
[8a] *Budker Institute of Nuclear Physics SB RAS, Novosibirsk 630090, Russia*
[8b] *Novosibirsk State University, Novosibirsk 630090, Russia*
[8c] *Novosibirsk State Technical University, Novosibirsk 630092, Russia*
[9] *University of California at Irvine, Irvine, California 92697, USA*
[10] *University of California at Riverside, Riverside, California 92521, USA*
[11] *University of California at Santa Cruz, Institute for Particle Physics, Santa Cruz, California 95064, USA*
[12] *California Institute of Technology, Pasadena, California 91125, USA*

[13]*University of Cincinnati, Cincinnati, Ohio 45221, USA*
[14]*University of Colorado, Boulder, Colorado 80309, USA*
[15]*Laboratoire Leprince-Ringuet, Ecole Polytechnique, CNRS/IN2P3, F-91128 Palaiseau, France*
[16a]*INFN Sezione di Ferrara, I-44122 Ferrara, Italy*
[16b]*Dipartimento di Fisica e Scienze della Terra, Università di Ferrara, I-44122 Ferrara, Italy*
[17]*INFN Laboratori Nazionali di Frascati, I-00044 Frascati, Italy*
[18]*INFN Sezione di Genova, I-16146 Genova, Italy*
[19]*Harvey Mudd College, Claremont, California 91711, USA*
[20]*Humboldt-Universität zu Berlin, Institut für Physik, D-12489 Berlin, Germany*
[21]*Indian Institute of Technology Guwahati, Guwahati, Assam 781 039, India*
[22]*University of Iowa, Iowa City, Iowa 52242, USA*
[23]*Iowa State University, Ames, Iowa 50011, USA*
[24]*Johns Hopkins University, Baltimore, Maryland 21218, USA*
[25]*Université Paris-Saclay, CNRS/IN2P3, IJCLab, F-91405 Orsay, France*
[26]*Lawrence Livermore National Laboratory, Livermore, California 94550, USA*
[27]*University of Liverpool, Liverpool L69 7ZE, United Kingdom*
[28]*Queen Mary, University of London, London E1 4NS, United Kingdom*
[29]*University of London, Royal Holloway and Bedford New College, Egham, Surrey TW20 0EX, United Kingdom*
[30]*University of Louisville, Louisville, Kentucky 40292, USA*
[31]*Johannes Gutenberg-Universität Mainz, Institut für Kernphysik, D-55099 Mainz, Germany*
[32]*University of Manchester, Manchester M13 9PL, United Kingdom*
[33]*University of Maryland, College Park, Maryland 20742, USA*
[34]*Massachusetts Institute of Technology, Laboratory for Nuclear Science, Cambridge, Massachusetts 02139, USA*
[35a]*Institute of Particle Physics, Montréal, Québec H3A 2T8, Canada*
[35b]*McGill University, Montréal, Québec H3A 2T8, Canada*
[36a]*INFN Sezione di Milano, I-20133 Milano, Italy*
[36b]*Dipartimento di Fisica, Università di Milano, I-20133 Milano, Italy*
[37]*University of Mississippi, University, Mississippi 38677, USA*
[38]*Université de Montréal, Physique des Particules, Montréal, Québec H3C 3J7, Canada*
[39]*INFN Sezione di Napoli and Dipartimento di Scienze Fisiche, Università di Napoli Federico II, I-80126 Napoli, Italy*
[40]*NIKHEF, National Institute for Nuclear Physics and High Energy Physics, NL-1009 DB Amsterdam, The Netherlands*
[41]*University of Notre Dame, Notre Dame, Indiana 46556, USA*
[42]*Ohio State University, Columbus, Ohio 43210, USA*
[43a]*INFN Sezione di Padova, I-35131 Padova, Italy*
[43b]*Dipartimento di Fisica, Università di Padova, I-35131 Padova, Italy*
[44]*Laboratoire de Physique Nucléaire et de Hautes Energies, Sorbonne Université, Paris Diderot Sorbonne Paris Cité, CNRS/IN2P3, F-75252 Paris, France*
[45a]*INFN Sezione di Perugia, I-06123 Perugia, Italy*
[45b]*Dipartimento di Fisica, Università di Perugia, I-06123 Perugia, Italy*
[46a]*INFN Sezione di Pisa, I-56127 Pisa, Italy*
[46b]*Dipartimento di Fisica, Università di Pisa, I-56127 Pisa, Italy*
[46c]*Scuola Normale Superiore di Pisa, I-56127 Pisa, Italy*
[47]*Princeton University, Princeton, New Jersey 08544, USA*
[48a]*INFN Sezione di Roma, I-00185 Roma, Italy*
[48b]*Dipartimento di Fisica, Università di Roma La Sapienza, I-00185 Roma, Italy*
[49]*Universität Rostock, D-18051 Rostock, Germany*
[50]*Rutherford Appleton Laboratory, Chilton, Didcot, Oxon OX11 0QX, United Kingdom*
[51]*IRFU, CEA, Université Paris-Saclay, F-91191 Gif-sur-Yvette, France*
[52]*SLAC National Accelerator Laboratory, Stanford, California 94309 USA*
[53]*University of South Carolina, Columbia, South Carolina 29208, USA*
[54]*Southern Methodist University, Dallas, Texas 75275, USA*
[55]*St. Francis Xavier University, Antigonish, Nova Scotia B2G 2W5, Canada*
[56]*Stanford University, Stanford, California 94305, USA*
[57]*State University of New York, Albany, New York 12222, USA*
[58]*Tel Aviv University, School of Physics and Astronomy, Tel Aviv 69978, Israel*
[59]*University of Tennessee, Knoxville, Tennessee 37996, USA*
[60]*University of Texas at Austin, Austin, Texas 78712, USA*
[61]*University of Texas at Dallas, Richardson, Texas 75083, USA*
[62a]*INFN Sezione di Torino, I-10125 Torino, Italy*
[62b]*Dipartimento di Fisica, Università di Torino, I-10125 Torino, Italy*

[63]*INFN Sezione di Trieste and Dipartimento di Fisica, Università di Trieste, I-34127 Trieste, Italy*
[64]*IFIC, Universitat de Valencia-CSIC, E-46071 Valencia, Spain*
[65a]*Institute of Particle Physics, Victoria, British Columbia V8W 3P6, Canada*
[65b]*University of Victoria, Victoria, British Columbia V8W 3P6, Canada*
[66]*Department of Physics, University of Warwick, Coventry CV4 7AL, United Kingdom*
[67]*University of Wisconsin, Madison, Wisconsin 53706, USA*

(Received 29 November 2019; revised manuscript received 22 January 2020; accepted 20 March 2020; published 16 April 2020)

A study of the two-body decays $B^{\pm} \to X_{c\bar{c}} K^{\pm}$, where $X_{c\bar{c}}$ refers to one charmonium state, is reported by the *BABAR* Collaboration using a data sample of 424 fb^{-1}. The absolute determination of branching fractions for these decays are significantly improved compared to previous *BABAR* measurements. Evidence is found for the decay $B^{+} \to X(3872) K^{+}$ at the 3σ level. The absolute branching fraction $\mathcal{B}[B^{+} \to X(3872) K^{+}] = [2.1 \pm 0.6(\text{stat}) \pm 0.3(\text{syst})] \times 10^{-4}$ is measured for the first time. It follows that $\mathcal{B}[X(3872) \to J/\psi \pi^{+} \pi^{-}] = (4.1 \pm 1.3)\%$, supporting the hypothesis of a molecular component for this resonance.

DOI: 10.1103/PhysRevLett.124.152001

In two-body B decays $B \to XK$, the X particle is predominantly a $c\bar{c}$ system with large available phase space. Many charmonium states are thus produced, with approximately equal rates when no strong selection rules apply [1]. They have mostly been observed using an exclusive reconstruction of the charmonium state $X_{c\bar{c}}$ [η_c, J/ψ, χ_{c1}, χ_{c2}, $\eta_c(2S)$, ψ'], with possibly the associated observation of the decay $B^{\pm} \to X_{c\bar{c}} K^{\pm}$ [2,3]. The exotic charmonium state $X(3872)$, also known as $\chi_{c1}(3872)$, has also been reconstructed in this way [4,5].

The determination of the absolute branching fraction $\mathcal{B}[B^{+} \to X(3872) K^{+}]$ leads to the absolute $\mathcal{B}[X(3872) \to J/\psi \pi^{+} \pi^{-}]$, bringing useful information regarding the complex nature of the $X(3872)$. The original tetraquark model [6] predicts this branching fraction to be about 50%. A more refined tetraquark model [7] can accommodate a much smaller branching fraction, but requires another particle, $X(3876)$, not yet observed. Various molecular models [8–10] predict this branching fraction to be $\lesssim 10\%$. Using the $X(3872)$ total width determination based on its line shape, or an upper limit on this quantity, information is provided on the partial width $\Gamma[X(3872) \to J/\psi \pi^{+} \pi^{-}]$, for which a wide range of predictions exist, from 1.3 MeV in the case of a pure charmonium state [11] to about 100 keV for molecular models [8].

In this Letter, we adopt a technique, pioneered by *BABAR* [12] and reused by Belle [13], based on the measurement in the B rest frame of the kaon momentum spectrum, where each two-body decay is identified by its monochromatic kaon. Taking advantage of the $\Upsilon(4S)$ decay to a $B\bar{B}$ meson pair, the B center-of-mass (c.m.) frame is determined event by event by fully reconstructing the other B meson. The branching fractions for the two-body decays $B^{\pm} \to X_{c\bar{c}} K^{\pm}$ can thus be measured independently of any *a priori* knowledge of the $X_{c\bar{c}}$ decay properties.

We use a data sample with an integrated luminosity of 424 fb^{-1} [14], collected with the *BABAR* detector at the PEP-II storage ring, at a c.m. energy corresponding to the $\Upsilon(4S)$ mass. Charged tracks are reconstructed with a five-layer silicon vertex tracker (SVT) and a 40-layer drift chamber (DCH), located in a 1.5 T magnetic field generated by a superconducting solenoidal magnet. The energies of photons and electrons are measured with a CsI(Tl) electromagnetic calorimeter. Charged hadron identification is performed using ionization measurements in the SVT and DCH and using a ring-imaging Čerenkov detector. The instrumented flux return of the solenoid is used to identify muons. A detailed description of the *BABAR* detector can be found in Refs. [15,16].

The analysis method is similar to that presented in Ref. [12]. The complete reconstruction of one of the two B mesons provides access to the rest frame of the other B meson. For signal events, two-body $B^{\pm}$ decays to $K^{\pm}X$, the kaon momentum in the B c.m. frame p_k exhibits a peak for each X particle, with mass $m_X = \sqrt{m_B^2 + m_K^2 - 2E_K m_B}$, where m_B and m_K are the masses of the B and K mesons and E_K is the kaon energy in the B rest frame. The p_k spectrum contains, besides a series of signal peaks, a background due to kaons from non-two-body decays or from decays of charmed mesons. We determine the observed number of each charmonium resonance $X_{c\bar{c}}$ from a fit to the kaon momentum distribution.

Event selection requires the reconstruction of a tagging $B^{\pm}$ meson (B tag) from $B \to SY$ decays, where the seed S is a fully reconstructed $D^{(*)0}$, $D^{(*)\pm}$, $D_s^{(*)\pm}$, or J/ψ meson, and Y represents a combination of $\pi^{\pm}$, $K^{\pm}$, π^{0}, and K_S^{0}

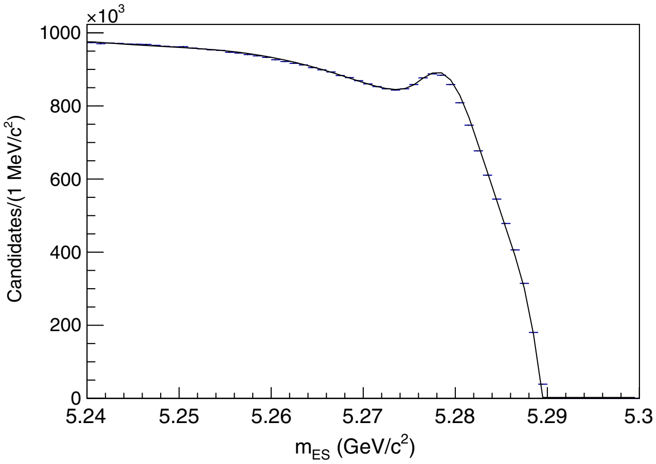

FIG. 1. The m_{ES} distribution of the exclusively reconstructed $B^{\pm}$, with the fit result superimposed.

hadrons [17]. For each mode, a purity [defined as $S/(S+B)$, where S is the number of signal events and B is the number of background events] larger than 0.08 is required. The number of B candidates is determined with a fit, shown in Fig. 1, to the distribution of the B-energy-substituted mass, $m_{\mathrm{ES}} = \sqrt{E_{\mathrm{c.m.}}^2/4 - p_B^2}$. Here, $E_{\mathrm{c.m.}}$ is the total c.m. energy, determined from the beam parameters, and p_B is the measured momentum of the reconstructed B in the $\Upsilon(4S)$ rest frame. The fit function is the sum of a Crystal Ball function [18] describing the signal and an ARGUS function [19] for the background. The number of fully reconstructed $B^{\pm}$ decays found by the fit is $1.65\times 10^6 \pm 4\times 10^3(\mathrm{stat}) \pm 6\times 10^4(\mathrm{syst})$. The systematic uncertainty is dominated by the background shape near the kinematic end point. This event yield is mentioned for reference but is not used in the determination of the branching ratios (BRs), except for the cross-check on $\mathrm{BR}(B^{\pm}\to J/\psi K^{\pm})$.

If more than one B candidate is found in an event, all candidates are retained. This is an important difference compared to Refs. [12,13], where only one candidate per event is retained. This method increases the efficiency and provides better decoupling between the signal and tag sides. Events not considered before, where the candidate selected as the best one was not the correct one, are now retained, including those where it belonged to the signal side. This point is important for the $X(3872)$ measurement because the probability to reconstruct a candidate from the signal side is enhanced for particles decaying to D mesons. The new method provides efficiency gains up to a factor of 3. The mean number of B-tag candidates per event is 1.85, and 39% of events have more than one candidate.

Event selection criteria are as follows: Each B-tag candidate should have $m_{\mathrm{ES}} > 5.275\,\mathrm{GeV}/c^2$ and be accompanied by an opposite-sign kaon candidate (charge conjugation is always implied), passing a tight particle identification selection. The pion contamination in this kaon sample is below 2%. A neural network (NN) is then used to suppress the continuum background. The inputs to the NN are seven variables related to the reconstructed B characteristics, its production kinematics, the topology of the full event, and the angular correlation between the reconstructed B and the rest of the event. The NN selection has an 80% efficiency for generic B^+B^- events and a factor 10 rejection against non-B background events coming from u, d, s, or c quark-antiquark pairs.

A second NN is used to reject secondary kaons produced in B-daughter D meson decays. This is a large background that increases rapidly with decreasing kaon momentum. In the B rest frame, the secondary kaons are embedded in the D decay products, which, given the boost of the D meson and its mass, are bounded in a cone and form a wide jet, whereas signal kaons recoil against a massive (3–4 GeV/c^2) state and tend to be more isolated, with the rest of the B decay products being more spherical. The input variables to this NN are the energy contained in a cone around the kaon track, the sphericity of the system recoiling against the kaon, the angle between the kaon and the thrust axis of the recoiling system, the minimum mass formed with the kaon, and the recoiling particles [20]. The two NNs are then combined in a single neural net, called super-NN, to optimize further the signal to background. Because of the non-negligible variation of the event topology with the mass of the charmonium particle, the super-NN is trained separately in the J/ψ and η_c signal region, and in the ψ' and $\eta_c(2S)$ region, with kaon background taken from simulation in the momentum ranges 1.6–1.9 and 1.2–1.5 GeV/c, respectively. The super-NN performance corresponds to a 72% signal efficiency at the $X(3872)$ peak and a background rejection factor varying between three in the $X(3872)$ and ψ' region to 4.5 in the J/ψ region.

To analyze the kaon momentum spectrum, we first determine the background shape and then perform a fit to the background-subtracted spectrum. The shape of the background spectrum is determined by interpolating through regions where no signal is expected, below 1.1 and above 1.9 GeV/c. Because the use of only these two regions leads to large uncertainty in the background parameters, we add data points in the two regions 1.34–1.36 and 1.53–1.57 GeV/c, where there is no peak, as indicated in Fig. 2.

Figure 2 also shows the fit to the simulated signal $K^{\pm}$ momentum spectrum for all charmonia peaks in the simulation. A good description is obtained when using, for each peak, a narrow Gaussian, whose width depends on momentum varying from 13 MeV/c for the J/ψ to 9 MeV/c for the ψ', and a two-piece Gaussian, 100 MeV/c wide on the left and 60 MeV/c wide on the right. A similar fit is performed for the $X(3872)$ with a dedicated Monte Carlo (MC) sample (Fig. 3). The narrow Gaussian width is measured to be 7 MeV/c and the wide Gaussian tails are 47 MeV/c on each side. All parameters

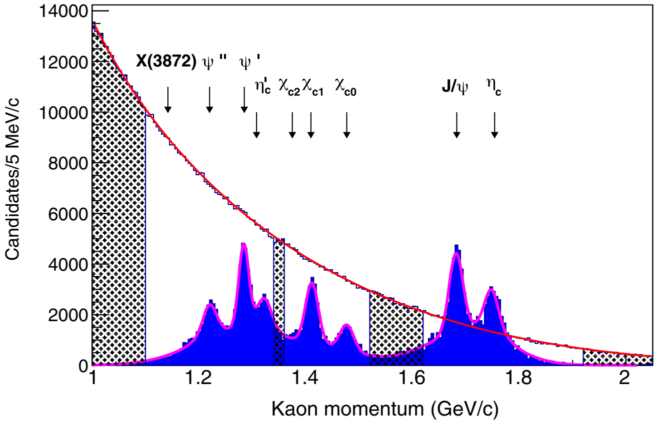

FIG. 2. The $K^{\pm}$ momentum spectrum for simulated events where no signal kaons are present. The MC statistics represent 3.5 times *BABAR* integrated luminosity. The hatched areas correspond to the zones used to fit the polynomial background. The filled blue histogram is the signal-only $K^{\pm}$ momentum spectrum in simulated events. The purple line represents the fit to this distribution.

describing the shapes of the signal peaks are fixed to these values in the fit to data. The wide Gaussian is associated with candidates where the B tag has a reconstructed $m_{\rm ES}$ in the signal region but is not built with the correct set of B decay products and, therefore, provides an incorrect boost. The presence of D mesons in $\psi(3770)$ or $X(3872)$ leads to a higher background under the B peak, leading to a large wide Gaussian component and a higher efficiency for the $X(3872)$: the MC efficiency is found to be $(48 \pm 2)\%$ and $(25 \pm 0.7)\%$ for J/ψ using the low and high mass training, respectively, $(51 \pm 2)\%$ for η_c, $(56 \pm 3)\%$ for χ_{c1}, $(61 \pm 3)\%$ for ψ', and $(77 \pm 2)\%$ for $X(3872)$.

When using the intermediate points to interpolate the background, the tails from the J/ψ and $\eta_c(2S)$ peaks extending into these intermediate regions are subtracted using the simulation with the known branching fractions [21]. The fit function is a product of fifth-order Chebyshev polynomials and an exponential function.

Small deviations are observed in the simulation between the background kaon momentum distribution and the fit function [20]. These defects in background shape do not affect the visibility of narrow peaks, such as that of the $X(3872)$ since the expected width of 7 MeV/c is much smaller than the ∼50 MeV/c typical width of the local deviations. The observed residuals in the 1.1–1.2 GeV/c region are corrected for, and the resulting uncertainty is taken into account.

The kaon spectrum between 1.5 and 2 GeV/c is expected to exhibit two peaks, one at $p_k = 1.684$ GeV/c corresponding to the J/ψ and a second at $p_k = 1.754$ GeV/c for the η_c. The super-NN is trained in the J/ψ–η_c region and the super-NN output is required to be > 0.85 with a B purity larger than 0.08. A fit to the background-subtracted spectrum is performed with the two signal functions determined above, the only free parameters being the charmonia yields. Figure 4 displays the results, with the yields $N_{J/\psi} = 2364 \pm 189$ and $N_{\eta_c} = 2259 \pm 188$. The statistical precision is 8%, a factor of about two improvement compared to Ref. [12].

The branching fraction $\mathcal{B}(B^{\pm} \to K^{\pm}\eta_c)$ is computed using the world average $\mathcal{B}(B^{\pm} \to K^{\pm}J/\psi)$ [21] and the ratio of the yields quoted above, to obtain

$$\mathcal{B}(B^{\pm} \to K^{\pm}\eta_c) = [0.96 \pm 0.12(\text{stat}) \pm 0.06(\text{syst}) \pm 0.03(\text{ref})] \times 10^{-3},$$

where the systematic uncertainty is detailed in Table I, and "ref" refers to the uncertainty in $\mathcal{B}(B^{\pm} \to K^{\pm}J/\psi)$ [21]. This result agrees with the world average $(1.09 \pm 0.09) \times 10^{-3}$ [21]. As a cross-check, $\mathcal{B}(B^{\pm} \to K^{\pm}J/\psi)$ is also extracted from the ratio of observed J/ψ events obtained

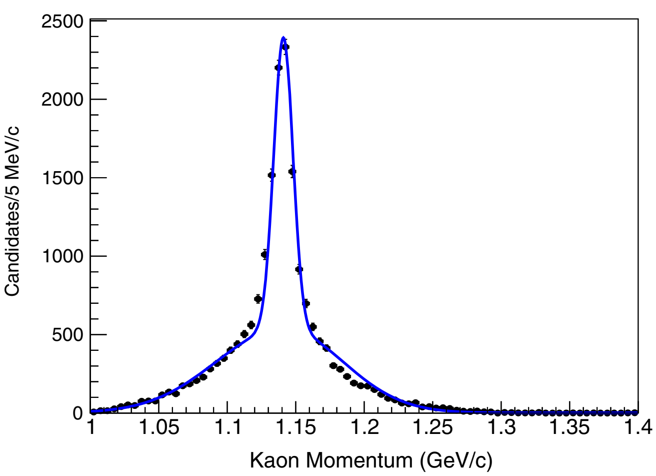

FIG. 3. Fit to the signal-only $K^{\pm}$ momentum spectrum in $X(3872)$ simulated events.

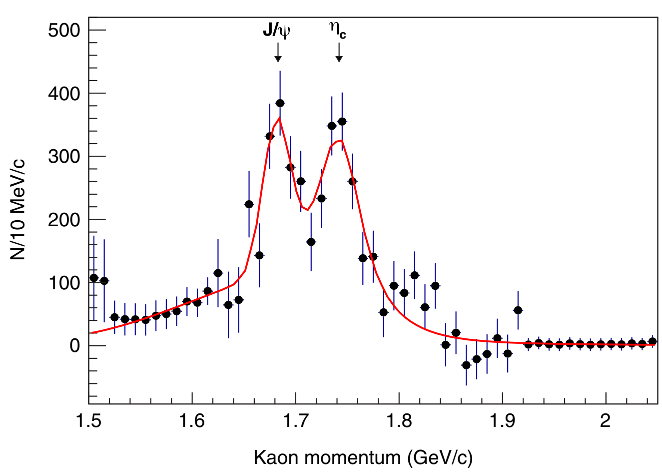

FIG. 4. The background-subtracted kaon momentum spectrum for data in the $J/\psi - \eta_c$ region with fit result superimposed.

TABLE I. Summary of relative systematic uncertainties (in percentage) for the η_c, χ_{c1}, $\eta_c(2S)$, ψ', and $X(3872)$ branching fractions, relative to $\mathcal{B}(B^{\pm} \to J/\psi K^{\pm})$.

Uncertainty source	η_c	χ_{c1}	$\eta_c(2S)$	ψ'	$X(3872)$
K identification	1	2	2	2	5
Decay model	···	···	1	···	5
Efficiency	0	2	2	2	5
p_K: peak position	2	2	8	2	2
p_K: signal narrow width	1	1	1	1	1
p_K: signal wide width	5	5	5	5	5
p_K: narrow width fraction	2	2	2	2	2
p_K: background shape	···	13	12	13	13
Decay width	1	···	1	···	···
Correction in signal-free regions	···	···	···	···	4
Total	6	14.5	15.1	14.6	16.3

in data and simulation: $\mathcal{B}(B^{\pm} \to K^{\pm} J/\psi) = [1.09 \pm 0.09(\text{stat}) \pm 0.06(\text{syst})] \times 10^{-3}$, in agreement with the world average.

The higher-mass region was blinded during the initial part of the analysis. Here, the super-NN is trained in the ψ' region and the super-NN output is required to be >0.6 with a B purity larger than 0.10. The p_K spectrum is fitted using the same procedure as above. The background shape is determined using a fit to the signal-free region after correction for the small residual signal in that region estimated from MC simulation. The kaon spectrum before (after) background subtraction is displayed in Fig. 5 (Fig. 6).

The fit to the background-subtracted signal spectrum (Fig. 6) is a sum of nine signal-peak functions corresponding to the $X(3872)$, $\psi(3770)$, ψ', $\eta_c(2S)$, χ_{c2}, χ_{c1}, χ_{c0}, J/ψ, and η_c. The peak locations are taken from Ref. [21] and the widths from fits to MC signal samples and include both

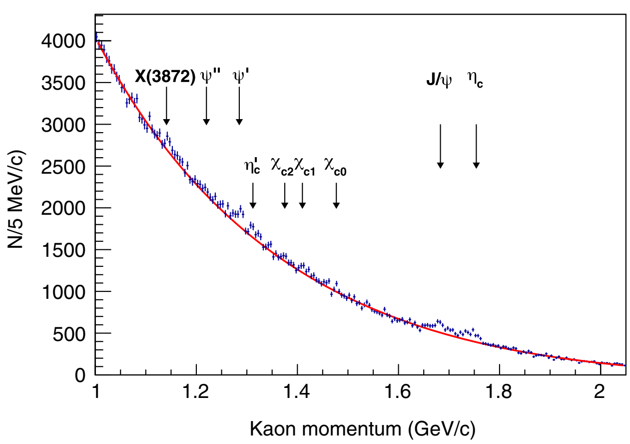

FIG. 5. The kaon momentum spectrum after applying final selection criteria and before background subtraction. The red line is the interpolated function describing the background shape. The arrows indicate the values at which a signal for each resonance is expected.

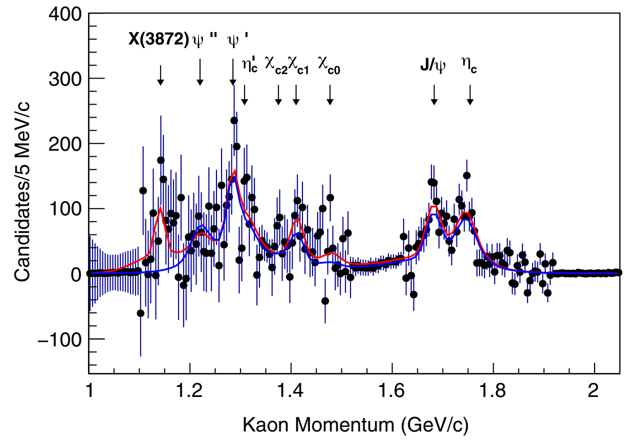

FIG. 6. The background-subtracted kaon momentum spectrum between 1 and 2.05 GeV/c. The fit function (red) includes signal peaks for nine particles, indicated by the arrows. The fit function where the $X(3872)$ yield is forced to zero is drawn in blue.

detector resolution and the natural width of each resonance. The peak labeled χ_{c1} refers to both χ_{c1} and h_c since these two states cannot be distinguished from each other in this analysis. A binned maximum likelihood fit is performed, with the nine charmonium yields as free parameters. Table II contains the fit results. Signal peaks are visible for η_c, J/ψ, χ_{c1}, ψ' [20], and $X(3872)$. A separate fit in which the $X(3872)$ signal is forced to zero has a χ^2 larger than that of the nominal fit by 11.1 units, which reduces to 9.0 when accounting for the uncertainty in the background shape in the 1.1–1.2 GeV/c region. Thus, there is 3σ evidence of the decay $B^{\pm} \to K^{\pm}\, X(3872)$, detected for the first time using this recoil technique.

Systematic uncertainties mainly stem from the imperfect description of the data by the simulation and are computed for the five particles having significance $>2\sigma$. An extra uncertainty is added for the $X(3872)$ for the limited knowledge of its decay modes.

TABLE II. Results from fits to the kaon momentum spectrum. $\mathcal{B}$ stands for the branching fraction for $B^{\pm} \to X_{c\bar{c}} K^{\pm}$. An additional 3% uncertainty must be added to these results, reflecting the present knowledge of the reference $\mathcal{B}(B^{+} \to J/\psi K^{+})$. The significance of each peak refers to the χ^2 increase of the fit when removing each resonance in turn.

Particle	Yield	$\mathcal{B}(10^{-4})$	N_σ
J/ψ	2364 ± 189	10.1 ± 0.29 (Ref. [21])	10.4
η_c	2259 ± 188	$9.6 \pm 1.2(\text{stat}) \pm 0.6(\text{syst})$	9.3
χ_{c0}	287 ± 181	$2.0 \pm 1.3(\text{stat}) \pm 0.3(\text{syst})$	1.6
χ_{c1}	1035 ± 193	$4.0 \pm 0.8(\text{stat}) \pm 0.6(\text{syst})$	2.2
χ_{c2}	200 ± 164	< 2.0	1.2
$\eta_c(2S)$	527 ± 271	$3.5 \pm 1.7(\text{stat}) \pm 0.5(\text{syst})$	2.3
ψ'	1278 ± 285	$4.6 \pm 1(\text{stat}) \pm 0.7(\text{syst})$	3.1
$\psi(3770)$	497 ± 308	$3.2 \pm 2.0(\text{stat}) \pm 0.5(\text{syst})$	1.2
$X(3872)$	992 ± 285	$2.1 \pm 0.6(\text{stat}) \pm 0.3(\text{syst})$	3.0

(i) Peak position: A deviation from the known peak position can induce an uncertainty in the number of events from the fit integral, estimated at 1%.

(ii) Signal shape: Four parameters are used to describe the signal shape: the main narrow width of the signal peak, the widths of the left- and right-hand side Gaussian tails, and the fraction under the narrow Gaussian. The uncertainty resulting from the uncertainty in the signal shape is estimated using the fit to the simulation sample containing only true kaons from two-body $B^{\pm}$ decays by comparing the fit results with the true numbers of events. When the resonance has a non-negligible natural width, as for the η_c, the uncertainty in this width is included.

(iii) Background subtraction: The statistical uncertainty of the background fit is propagated, including correlations, into the statistical uncertainty and is not a systematic uncertainty. The systematic uncertainties stem from different background parametrizations and from the correction due to the signal subtraction in the 1.1–1.2 GeV/c region. This latter uncertainty is determined as the change to the $X(3872)$ yield introduced by a one-sigma deviation of the correction function.

(iv) Efficiency determination: Uncertainties in detection efficiency arise in the kaon reconstruction and particle identification and in the super-NN-based selection. These uncertainties cancel to a good approximation in the ratios of the branching fractions of all resonances to the J/ψ.

(v) $X(3872)$ decay model: The signal shape is not the same for DD and $J/\psi X$ decays and this effect induces a small change in the signal yield in the fit. Varying the ratio between these two types of decays leads to a 5% additional uncertainty.

Table I summarizes the various systematic uncertainties, and Table II summarizes the branching fraction results.

The number of $X(3872)$ events is converted into an absolute branching fraction using the number of observed J/ψ events, its absolute branching fraction, and the relative efficiency ratio, with the result $\mathcal{B}[B^+ \to X(3872)K^+] = [2.1 \pm 0.6(\text{stat}) \pm 0.3(\text{syst}) \pm 0.1(\text{ref})] \times 10^{-4}$. Using the measured product branching fraction $\mathcal{B}[B^+ \to X(3872)K^+] \times \mathcal{B}[X(3872) \to J/\psi\pi^+\pi^-] = (8.6 \pm 0.8) \times 10^{-6}$ [21], this translates into $\mathcal{B}[X(3872) \to J/\psi\pi^+\pi^-] = (4.1 \pm 1.3)\%$. From this, an upper limit on the partial width $\Gamma[X(3872) \to J/\psi\pi^+\pi^-]$ can be set in the 100 keV range, using 3 MeV as an upper limit for the $X(3872)$ total width, as measured in its DD decay channel [22,23]. Our measurement therefore suggests that the $X(3872)$ has a significant molecular component.

We report an update to our first analysis [12] with the full *BABAR* statistics. Two new features are introduced: the inclusion of all B candidates has led to an increase of efficiency and a better separation between signal and tag sides of an event; the fit to a polynomial background in regions where no signal is present reduces the statistical and systematic uncertainties related to the background subtraction. We obtain the following results:

$$\mathcal{B}(B^+ \to \eta_c K^+) = [0.96 \pm 0.12(\text{stat}) \pm 0.06(\text{syst}) \pm 0.03(\text{ref})] \times 10^{-3},$$

$$\mathcal{B}[B^+ \to X(3872)K^+] = [2.1 \pm 0.6(\text{stat}) \pm 0.3(\text{syst}) \pm 0.1(\text{ref})] \times 10^{-4},$$

$$\mathcal{B}[X(3872) \to J/\psi\pi^+\pi^-] = (4.1 \pm 1.3)\%.$$

This result will certainly contribute to the determination of the complex nature of the $X(3872)$ particle.

We are grateful for the extraordinary contributions of our PEP-II2 colleagues in achieving the excellent luminosity and machine conditions that have made this work possible. The success of this project also relies critically on the expertise and dedication of the computing organizations that support *BABAR*. The collaborating institutions wish to thank SLAC for its support and the kind hospitality extended to them. This work is supported by the U.S. Department of Energy and National Science Foundation, the Natural Sciences and Engineering Research Council (Canada), Institute of High Energy Physics (China), the Commissariat à l'Energie Atomique and Institut National de Physique Nucléaire et de Physique des Particules (France), the Bundesministerium für Bildung und Forschung and Deutsche Forschungsgemeinschaft (Germany), the Istituto Nazionale di Fisica Nucleare (Italy), the Foundation for Fundamental Research on Matter (The Netherlands), the Research Council of Norway, the Ministry of Science and Technology of the Russian Federation, and the Particle Physics and Astronomy Research Council (United Kingdom). Individuals have received support from CONACyT (Mexico), the A. P. Sloan Foundation, the Research Corporation, and the Alexander von Humboldt Foundation.

[*]Deceased.
[†]Now at Wuhan University, Wuhan 430072, China.
[‡]Now at Università di Bologna and INFN Sezione di Bologna, I-47921 Rimini, Italy.
[§]Now at University of Huddersfield, Huddersfield HD1 3DH, United Kingdom.
[∥]Now at University of South Alabama, Mobile, Alabama 36688, USA.
[¶]Also at Università di Sassari, I-07100 Sassari, Italy.
[**]Also at Gran Sasso Science Institute, I-67100 LAquila, Italy.

[1] C. Quigg, Frascati Phys. Ser. **34**, 393 (2004), and references therein.
[2] B. Aubert *et al.* (*BABAR* Collaboration), Phys. Rev. D **67**, 032002 (2003).
[3] S. K. Choi *et al.* (Belle Collaboration), Phys. Rev. Lett. **89**, 102001 (2002).
[4] S. K. Choi *et al.* (Belle Collaboration), Phys. Rev. D **84**, 052004 (2011).

[5] B. Aubert *et al.* (*BABAR* Collaboration), Phys. Rev. D **77**, 111101 (2008).
[6] L. Maiani, F. Piccinini, A. D. Polosa, and V. Riquer, Phys. Rev. D **71**, 014028 (2005).
[7] L. Maiani, A. D. Polosa, and V. Riquer, Phys. Rev. Lett. **99**, 182003 (2007).
[8] E. Braaten, and M. Kusunoki, Phys. Rev. D **72**, 054022 (2005).
[9] T. Barnes and S. Godfrey, Phys. Rev. D **69**, 054008 (2004).
[10] P. G. Ortega and E. R. Arriola, Chin. Phys. C **43**, 124107 (2019).
[11] E. Swanson, Phys. Lett. B **588**, 189 (2004).
[12] B. Aubert *et al.* (*BABAR* Collaboration), Phys. Rev. Lett. **96**, 052002 (2006).
[13] Y. Kato *et al.* (Belle Collaboration), Phys. Rev. D **97**, 012005 (2018).
[14] J. P. Lees *et al.* (*BABAR* Collaboration), Nucl. Instrum. Methods Phys. Res., Sect. A **726**, 203 (2013).
[15] B. Aubert *et al.* (*BABAR* Collaboration), Nucl. Instrum. Methods Phys. Res., Sect. A **479**, 1 (2002).
[16] B. Aubert *et al.* (*BABAR* Collaboration), Nucl. Instrum. Methods Phys. Res., Sect. A **729**, 615 (2013).
[17] B. Aubert *et al.* (*BABAR* Collaboration), Phys. Rev. Lett. **109**, 101802 (2012).
[18] T. Skwarnicki *et al.*, Report No. DESY-F31-86-02.
[19] H. Albrecht *et al.* (ARGUS Collaboration), Phys. Lett. B **318**, 397 (1993).
[20] See Supplemental Material at http://link.aps.org/supplemental/10.1103/PhysRevLett.124.152001 for the performance of the topological NN (Fig. 1), for the distribution of the residues to the fit in MC, as function of kaon momentum (Fig. 2), for the analysis results, when optimized in the $\psi' - \eta_c(2S)$ region, as function of momentum (Fig. 3), and of recoil mass (Fig. 4).
[21] M. Tanabashi *et al.* (Particle Data Group), Phys. Rev. D **98**, 030001 (2018); and 2019 update.
[22] B. Aubert *et al.* (*BABAR* Collaboration), Phys. Rev. D **77**, 011102 (2008).
[23] T. Aushev *et al.* (Belle Collaboration), Phys. Rev. D **81**, 031103 (2010).